

Identifying the SN 2022acko progenitor with *JWST*

Schuyler D. Van Dyk,¹★ K. Azalee Bostroem,²† Jennifer E. Andrews,³ Yize Dong,⁴
 Alexei V. Filippenko,⁵ Ori D. Fox,⁶ Emily Hoang,⁴ Griffin Hosseinzadeh,² Daryl Janzen,⁷
 Jacob E. Jencson,⁸ Michael J. Lundquist,⁹ Nicolas Meza,⁴ Dan Milisavljevic,^{10,11}
 Jeniveve Pearson,² David J. Sand,² Manisha Shrestha,² Stefano Valenti,⁴ D. Andrew Howell^{12,13}

¹Caltech/IPAC, Mailcode 100-22, Pasadena, CA 91125, USA

²Steward Observatory, University of Arizona, 933 North Cherry Avenue, Tucson, AZ 85721, USA

³Gemini Observatory/NSF’s NOIRLab, 670 N. A’ohoku Place, Hilo, HI 96720, USA

⁴Department of Physics and Astronomy, University of California, Davis, 1 Shields Avenue, Davis, CA 95616-5270, USA

⁵Department of Astronomy, University of California, Berkeley, CA 94720-3411, USA

⁶Space Telescope Science Institute, 3700 San Martin Drive, Baltimore, MD 21218, USA

⁷Department of Physics & Engineering Physics, University of Saskatchewan, 116 Science Pl, Saskatoon, SK S7N 5E2, Canada

⁸Department of Physics and Astronomy, The Johns Hopkins University, Baltimore, MD 21218, USA

⁹W.M. Keck Observatory, 65-1120 Mamalahoa Highway, Kamuela, HI 96743, USA

¹⁰Department of Physics and Astronomy, Purdue University, 525 Northwestern Avenue, West Lafayette, IN 47907, USA

¹¹Integrative Data Science Initiative, Purdue University, West Lafayette, IN 47907, USA

¹²Las Cumbres Observatory, 6740 Cortona Dr. Suite 102, Goleta, CA, 93117, USA

¹³Physics Department, University of California, Santa Barbara, Santa Barbara, CA, 93111, USA

Accepted XXX. Received YYY; in original form ZZZ

ABSTRACT

We report analysis using the *James Webb Space Telescope (JWST)* to identify a candidate progenitor star of the Type II-plateau supernova SN 2022acko in the nearby, barred spiral galaxy NGC 1300. To our knowledge, our discovery represents the first time *JWST* has been used to localize a progenitor system in pre-explosion archival *Hubble Space Telescope (HST)* images. We astrometrically registered a *JWST* NIRCcam image from 2023 January, in which the SN was serendipitously captured, to pre-SN *HST* F160W and F814W images from 2017 and 2004, respectively. A star corresponding precisely to the SN position has been isolated with reasonable confidence, although a $\sim 2.9\sigma$ difference exists between the measured position for the star from *HST* and the transformed SN position from *JWST*. That star has a spectral energy distribution and overall luminosity consistent with a single-star model having an initial mass somewhat less than the canonical $8 M_{\odot}$ theoretical threshold for core collapse, although the star’s initial mass is inconsistent with that of a super-asymptotic giant branch star which might be a forerunner of an electron-capture SN. The properties of the progenitor alone imply that SN 2022acko is a relatively normal SN II-P, albeit most likely a low-luminosity one. The progenitor candidate should be confirmed with follow-up *HST* imaging at late times, when the SN has sufficiently faded. This potential use of *JWST* opens a new era of identifying SN progenitor candidates at high spatial resolution.

Key words: supernovae: general – supernovae: SN 2022acko – stars: massive – stars: evolution

1 INTRODUCTION

Supernovae (SNe) are the catastrophic endpoints of the lives of some stars. It is widely believed that the total disruption of a white dwarf (WD), as a consequence of critical mass accretion from a dwarf or giant star (or a merger with another WD), leads to thermonuclear explosion as normal Type Ia SNe, which have proven to be highly valuable cosmological probes owing to their high, standardizable luminosity. Stars with initial masses $M_{\text{ini}} \geq 8 M_{\odot}$ reach a point in their evolution at which nuclear burning can no longer support the

inner core, and the collapse of the core to neutron degeneracy rapidly leads to the explosive removal of the outer stellar envelope — a core-collapse SN (CCSN; e.g., Woosley & Weaver 1986). CCSNe account for $\sim 76\%$ of all SNe locally (Li et al. 2011; Graur et al. 2017). CCSNe are not homogeneous in their properties: both spectroscopically and photometrically they roughly divide further into the H-rich Type II and the H-poor Type Ib and Ic, with Type IIb constituting an intermediate grouping (see, e.g. Filippenko 1997; Gal-Yam 2017, for reviews of SN classification). Type II SNe have been classically separated into the Type II-plateau (II-P) and II-linear (II-L), based on their light-curve properties, although such distinctions in the modern view are debatable (Anderson et al. 2014; Valenti et al. 2016). Further subdivisions have emerged among the SNe II, Ib, and Ic with respect

★ E-mail: vandyk@ipac.caltech.edu (SVD)

† LSSTC Catalyst Fellow

to the presence of relatively narrow spectral emission features (the so-called “n” subtypes), interpreted as being indicative of the presence of dense circumstellar material.

Of utmost importance in understanding SNe in general, and CC-SNe specifically, is mapping the various SN subtypes to classes of progenitor star. A number of indirect methods have been employed, but the most direct approach is to identify the actual star that has exploded. The lion’s share of such detections have been made in pre-explosion *Hubble Space Telescope* (*HST*) archival images. As a community, we have successfully demonstrated in more than 20 cases that SNe II-P, in particular, arise from massive stars in the red supergiant (RSG) phase, as expected theoretically (Smartt et al. 2009; Smartt 2015; Van Dyk 2017). The RSGs are likely in a limited range of M_{ini} , the low end at the core-collapse limit and $\lesssim 17 M_{\odot}$ at the high end (although see Davies & Beasor 2020). SNe IIn appear to arise potentially from a higher-mass stellar group, with remarkable outbursts observed before explosion, ostensibly as luminous blue variable stars (e.g., Gal-Yam & Leonard 2009; Smith et al. 2022; Brennan et al. 2022; Jencson et al. 2022). For SNe Ib, a hot He-star progenitor was identified for one event (iPTF13bvn; e.g., Eldridge & Maund 2016), whereas a cool, extended star was identified for another (SN 2019yvr; Kilpatrick et al. 2021). A potentially hot, luminous candidate progenitor has been isolated for one SN Ic (SN 2017ein; Van Dyk et al. 2018; Kilpatrick et al. 2018; Xiang et al. 2019), although this remains to be confirmed.

The most prevalent CCSNe, SNe II-P ($\sim 48\%$ locally; Smith et al. 2011), are themselves also quite heterogeneous, most notably with a range in both peak and overall luminosities, as well as plateau duration (e.g., Anderson et al. 2014; Valenti et al. 2016; de Jaeger et al. 2019). At the low-luminosity end, the RSG progenitors have all been found to be at the lower end of the M_{ini} range, such as SN 2005cs ($9_{-2}^{+3} M_{\odot}$, Maund et al. 2005; $10 \pm 3 M_{\odot}$, Li et al. 2006), SN 2008bk ($8\text{--}8.5 M_{\odot}$, Van Dyk et al. 2012; $8\text{--}10 M_{\odot}$, O’Neill et al. 2021), and SN 2018aoq ($\sim 10 M_{\odot}$, O’Neill et al. 2019). For a nominal local Universe initial-mass function, we would expect lower-mass progenitors and, thus, low-luminosity SNe II to predominate in number. What makes this of critical interest is that these low masses are very near the expected boundaries between WD formation and core collapse, as well as the intermediate scenario of electron-capture (EC) explosions of super-asymptotic giant branch (AGB) stars with O-Ne-Mg cores (e.g., Miyaji et al. 1980; Nomoto 1984; Doherty et al. 2017). The recent case of SN 2018zd has brought this potential fine line to the fore: Hiramatsu et al. (2021) claimed, based on the SN’s properties, this SN was the first *bona fide* example of an ECSN, whereas Zhang et al. (2020) argued that SN 2018zd had properties more consistent with those of normal SNe II-P. Both studies characterised the identified progenitor candidate as potentially being a super-AGB (SAGB) star (Van Dyk et al. 2023 has since confirmed the candidate as the progenitor). Nevertheless, probing where these boundaries exist and what factors govern them is a key area of exploration in our understanding of stellar astrophysics and evolution. Garnering further examples of low-luminosity SNe II-P and their progenitors is therefore important and welcome.

Here we present the identification of the progenitor of the SN II-P 2022acko. The precise locations of previous SNe in archival images have been established either using *HST* or adaptive-optics ground-based observations of the SN itself. In this case, to our knowledge for the *first time*, we employ the novel method of pinpointing SN 2022acko in pre-SN *HST* data via *JWST* images containing the SN. SN 2022acko was first discovered on 2022 December 6 (UTC dates are used throughout this paper) at 16.5 mag, $58^{\circ}2$ north and $29^{\circ}6$ west of the nucleus of NGC 1300 (Lundquist et al. 2022), by the

Distance Less Than 40 Mpc (DLT40) survey (Tartaglia et al. 2018). It was classified the following day as a young SN II-P (Li et al. 2022). The SN is also known as DLT22v, ATLAS22bnms, ZTF22abyivoq, PS22mpv, and Gaia23aap. A detailed description of the SN at early times, including analysis of *HST* ultraviolet spectroscopy, will be presented by K. A. Bostroem et al. (2023, in prep.); they find that it is most consistent with a low-luminosity SN II-P. SN 2022acko is, as far as we know, the first historical SN to be discovered in this nearby, nearly face-on barred spiral galaxy.

2 OBSERVATIONS AND REDUCTIONS

2.1 *HST* data

The site of SN 2022acko was serendipitously covered in various *HST* observations of the host galaxy by several different programs. We obtained all of these publicly available data from the Mikulski Archive for Space Telescopes (MAST). The first set of data was obtained with the now-decommissioned Wide-Field and Planetary Camera 2 (WFPC2) on 2001 January 6 (21.9 yr before explosion) in F606W by program GO-8597 (PI M. Regan). The second set was obtained with the Advanced Camera for Surveys in the Wide Field Channel (ACS/WFC) on 2004 September 21 (18.2 yr) in F435W, F555W, F658N, and F814W by GO/DD-10342 (PI K. Noll; these were “Hubble Heritage” observations); note that only the “NGC1300-POS1” field contains the relevant half of the galaxy with the SN site. Next, the host galaxy was observed with the Wide-Field Camera 3 IR channel (WFC3/IR) on 2017 October 27 (5.1 yr) in F160W by GO-15133 (PI P. Erwin). Observations were also obtained with the WFC3 UVIS channel (WFC3/UVIS) in F475W and F814W; however, these were in subarray mode, centered on the nucleus, so they missed the SN site. Finally, WFC3/UVIS observations were conducted, in full-array mode, on 2020 January 4 (2.9 yr) in F275W and F336W by GO-15654 (PI J. Lee; PHANGS-HST, Lee et al. 2022b). We show portions of the image mosaics in F814W and F160W, containing the SN site, in Figure 1.

2.2 *JWST* data

The host galaxy was also observed on 2023 January 25, just 52 d after explosion, using *JWST* with both the NIRCcam and MIRI instruments by program GO-2107 (PI J. Lee; PHANGS-JWST, Lee et al. 2022a). The bands used for NIRCcam in both the short- and long-wavelength channels were F200W (9620 s), F300M (773 s), F335M (773 s), and F360M (859 s), whereas for MIRI, the bands were F770W, F1000W, F1130W, and F2100W. We obtained these publicly available data as Level-3 mosaics from MAST as soon as they appeared. The focus of this paper is on utilising the NIRCcam data for the purpose of potentially identifying the SN progenitor, since those bands match up best in wavelength and at comparable spatial resolution with the available *HST* bands, whereas the MIRI images do not meet these stipulations. We will therefore not be analyzing the MIRI data here at all.

The point-spread-function (PSF) profile of the SN in F200W, unfortunately, appears hopelessly saturated, as a result of the SN’s brightness and exposure depth of the observations in that band, making it worthless for our purpose. On the contrary, the PSF was of high quality in the remaining medium bands. The first three medium bands are intended to sample various molecular emission features from components in the interstellar medium (water ice, PAHs/CH₄), and the fourth band is intended for continuum emission from brown

dwarfs and planets. Nebular emission is apparent in the images in those first three bands; however, we selected F300M for use here, rather than the continuum band (F335W); any ice emission features in the data do not appear to be particularly strong, such that most of the observed flux in the image appears to arise from point sources. Furthermore, F300M is the one closest in wavelength to the reddest *HST* band (F160W). We show a portion of the image mosaic in F300M, containing the SN, in Figure 1.

2.3 Spitzer data

Archival data containing the SN site from the post-cryogenic *Spitzer Space Telescope* mission are publicly available from the NASA/IPAC Infrared Science Archive (IRSA), via the *Spitzer* Heritage Archive. These data are in the 3.6 and 4.5 μm bands on 2009 October 4 (13.2 yr) from program 61009 (PI W. Freedman) and 2009 September 5 (13.3 yr) and October 10 (13.2 yr) from program 61065 (PI K. Sheth).

2.4 Astrometry and photometry

In order to perform the necessary relative astrometry and determine which star, if any, could be considered a progenitor candidate, we first selected 20 relatively isolated stars in common spread spatially across the mosaics in both *HST* F160W and *JWST* F300M. We carefully eliminated consideration of any objects in the mosaics that were extended and did not have a clean stellar PSF profile. Using the task *geomap* within PyRAF with second-order fitting, we were able to align the two mosaics with a formal 1σ root-mean-square (rms) uncertainty in the mean astrometry of 0.09 WFC3/IR pixel (or ~ 12 mas). As mentioned above, the PSF of the SN itself in the F300M mosaic was very stellar-like, and we could therefore accurately measure its position in those *JWST* data and transform its position with the task *geoxytran* to the F160W mosaic. Doing so, we were able to isolate the star as indicated in Figure 1 (middle panel). We note, however, that the difference between the pixel position transformed from *JWST* and the position measured from the F160W mosaic itself is 0.26 WFC3/IR pixel, which is a difference of $\sim 2.9\sigma$. We performed a similar alignment between the F814W and F300M mosaics, based on 15 stars in common, and obtain a rms uncertainty in the registration of 0.10 UVIS pixel and a positional offset between the measured position and the transformed one of 0.52 pixel, a $\sim 5.2\sigma$ difference. Similarly, we associated the detected star at F814W indicated in Figure 1 (left panel) with the SN. Furthermore, we consider it highly likely that the F160W and F814W detections are of the same star. The positional offsets, however, are somewhat disconcerting, yet no other source appears to exist at F160W or F814W closer to the transformed positions. We further note that the PSF of the object at both F160W and F814W appears stellar-like, although at the detection level for the star in both bands (see below), measuring an accurate centroid for the PSF was not straightforward. At the assumed distance to the host (see below) we cannot rule out that it is a blend or a compact star cluster (the 1.84-pixel full-width at half maximum, FWHM, of the PSF at F160W corresponds at that distance to ~ 22 pc). Nevertheless, we proceed from this point assuming that this object is the SN progenitor candidate; of course, it remains to be confirmed that this is indeed the progenitor when the candidate is shown to have vanished (e.g., Van Dyk et al. 2023).

The *HST* WFPC2, ACS/WFC, and WFC3/UVIS data were mosaicked per band using *Astrodrizzle* (STScI Development Team 2012). In the case of WFC3/IR both the pipeline-drizzled “drz” mosaic and the individual “flt” frames obtained from MAST were

Table 1. Photometry of the SN 2022acko progenitor candidate.

Band	Mag ^a
F275W	> 25.2
F336W	> 26.0
F435W	> 27.8
F555W	> 27.0
F606W	> 26.0
F658N	> 24.7
F814W	25.61(09)
F160W	22.88(07)

^aMagnitudes are in the Vega system, and uncertainties of hundredths of a mag are in parentheses; upper limits are 5σ .

utilised. Similarly, we obtained the pipeline-produced *JWST* NIR-Cam “i2d” mosaic directly from the archive. As a by-product of running *Astrodrizzle* on the *HST* data, cosmic-ray (CR) hits on the detectors are masked in the data-quality array for each frame. The frames for each of the various *HST* bands were then run through PSF-fitting photometry using *Dolphot* (Dolphin 2016), with the mosaic in one band serving as the source detection reference. *Dolphot* input parameters were set at FitSky=3, RAper=8, and InterpPSFlib=1, with further charge-transfer efficiency (CTE) correction set to zero (except for the one WFPC2 dataset). The CR-hit flagging is important, in particular, for the aperture-correction measurements on each frame. The photometric results from *Dolphot* are returned as Vega magnitudes, and we present these in Table 1.

The star is detected only in F814W and F160W. We note that the F160W detection is at a formal signal-to-noise ratio (S/N) of 15.3, and the F814W detection is at S/N = 12.1. The star was not detected in any of the other bands. Instead, we provide upper brightness limits on detection in these bands. Here we set these limits at the formal S/N = 5 returned by *Dolphot* (following Van Dyk et al. 2023, but see the limitations and caveats associated with this assumption).

For the *Spitzer* data we combined all of the artefact-corrected basic calibrated data (BCD) in each band and mosaicked these frames using MOPEX (Makovoz & Khan 2005). PSF-fitting photometry was also executed on the individual frames using APEX (Makovoz & Marleau 2005). No source was visibly detected at the relatively uncrowded SN site in the resulting mosaics (not shown). From the photometry we considered the faintest detected source nearest the SN site in each band, in order to place upper limits on detection of the progenitor: these were at flux densities of 13.87 and 10.55 μJy at 3.6 and 4.5 μm , respectively.

3 THE SN 2022acko PROGENITOR

The next step is to interpret the photometry by building a spectral energy distribution (SED) for the progenitor candidate. This is reasonably straightforward to do, in that we only have two photometric detections along with many upper limits. For lack of any other reliable distance indicator, we adopt a distance to the host galaxy of 18.99 ± 2.85 Mpc (distance modulus $\mu = 31.39 \pm 0.33$ mag) that Anand et al. (2021) estimated from the Numerical Actions Method (NAM; Shaya et al. 2017). As far as extinction to SN 2022acko, from an analysis of the Na I D line profiles in an early-time moderate-resolution spectrum, Bostroem et al. (in prep.) measured essentially the same equivalent width for a component associated internally to the host as a component associated with the Galactic foreground. The foreground visual extinction is $A_V = 0.083$ mag, so we assume

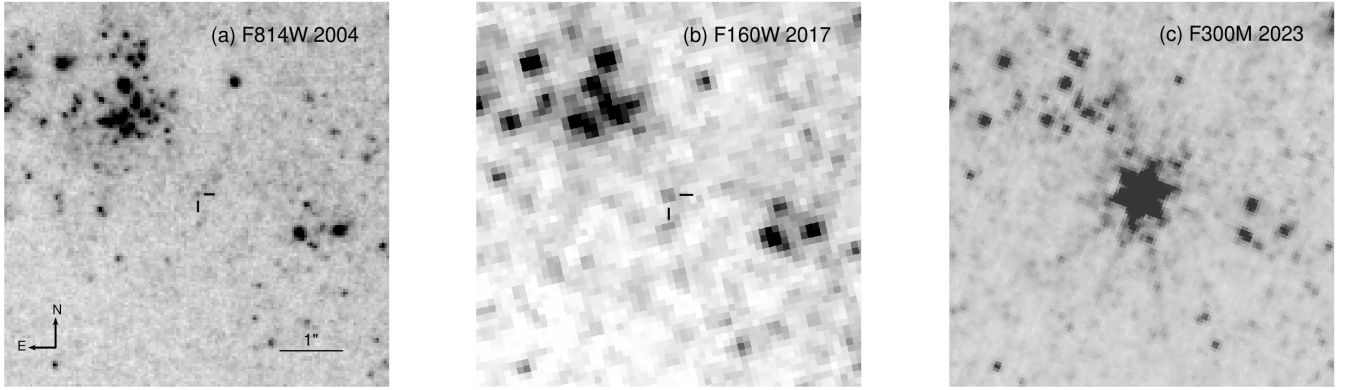


Figure 1. *Left:* A portion of a *HST* WFC3/UVIS image mosaic in F814W from 2004 September 21, with the progenitor candidate for SN 2022acko indicated with tick marks. *Middle:* same as the left panel, but for a WFC3/IR F160W mosaic from 2017 October 27. *Right:* a portion of a *JWST* NIRCcam mosaic in F300M from 2023 January 25. All panels are shown at the same scale and orientation. North is up and east is to the left.

here that the total extinction, $A_V(\text{tot})$, is equivalent simply to doubling the foreground value: $A_V(\text{tot}) \approx 0.166$ mag. Bostroem et al. estimated a slightly higher value, 0.205 mag, but this difference is not particularly critical.

Correcting the observed photometry for the distance and extinction, assuming an interstellar reddening law with $R_V = 3.1$, results in the SED for the progenitor candidate shown in Figure 2. The uncertainties in the F814W and F160W data arise from the uncertainty in the distance modulus, the photometric uncertainties, and the difference in the assumed extinctions between Bostroem et al. and this study, all added in quadrature; the total 1σ uncertainties are overwhelmingly driven by the uncertainty in the distance.

The final step, then, is to model the observed SED. We consider recent single-star evolutionary models from BPASS (the Binary Population and Spectral Synthesis code, v2.2.2; Stanway & Eldridge 2018). For lack of observational evidence to the contrary, we assume models at solar metallicity, which is nominally consistent with the ~ 7 kpc distance of the SN site from the host nucleus. Little motivation exists to consider binary evolutionary models here, since the available evidence for low-luminosity SN II-P progenitors being in binary systems (perhaps other than in wide, noninteractive binaries; e.g., O’Neill et al. 2019) is scant. We show in Figure 2 the end-points of three models at slightly different values of M_{ini} : 8, 7.7, and 7.6 M_{\odot} . (Note that the termini of the BPASS models is the end of carbon burning.) As can be seen in the figure, the upper limits on the SED are not particularly constraining. The 8 M_{\odot} model, an RSG with effective temperature $\log T_{\text{eff}}/\text{K} = 3.544$, bolometric luminosity $\log(L_{\text{bol}}/L_{\odot}) = 4.454$, and radius $R = 459 R_{\odot}$ appears to be too luminous in F814W. The 7.7 M_{\odot} model, with $\log T_{\text{eff}}/\text{K} = 3.552$, $\log(L_{\text{bol}}/L_{\odot}) = 4.304$, and $R = 372 R_{\odot}$ is a better comparison, although it is slightly beyond the 1σ uncertainty in F814W. For the 7.6 M_{\odot} model, the transition from massive RSG to SAGB has occurred, according to BPASS; this model SED has a markedly different shape and total luminosity (with $\log(T_{\text{eff}}/\text{K}) = 3.475$, $\log(L_{\text{bol}}/L_{\odot}) = 5.047$, and $R = 1247 R_{\odot}$) than do the RSG models and provides overall a very poor fit to the observations.

Note that we have not included circumstellar dust for any of these models, particularly the RSGs, primarily since little evidence exists that such dust is important for RSGs at this low M_{ini} (e.g., Massey et al. 2005; O’Neill et al. 2019, 2021). We also cannot be certain that the presumed SAGB does not have at least some circumstellar dust as well (e.g., Dell’Agli et al. 2017). However, it is possible that

some RSG progenitors may experience outbursts prior to explosion that may result in obscuring material that could “hide” the progenitor from detection, although such outbursts are predicted to occur < 1 yr prior to the SN (Davies et al. 2022; none of the archival *HST* or *Spitzer* data were obtained that soon before explosion). We consider the *Spitzer* upper limits, above, and the implications for the possibility of an undetected SN 2022acko progenitor detection, neighboring the candidate within its PSF. These limits are > 18.3 and > 18.1 mag at 3.6 and 4.5 μm , respectively¹. At the host distance (and with negligible extinction), these correspond to absolute brightnesses of > -13.1 and > -13.3 mag, respectively (not shown in Figure 2). Note that the luminous, dusty progenitor of SN 2017eaw (e.g., Van Dyk et al. 2019, 2023) had absolute brightnesses of -11.46 and -11.67 mag in the two respective bands. If there were a dusty progenitor for SN 2022acko, it would have required ≥ 1 mag circumstellar dust extinction than did the progenitor of SN 2017eaw, in order to evade detection in *Spitzer*; such dust would likely have been destroyed during the SN explosion.

4 DISCUSSION AND CONCLUSIONS

We have, for the first time, identified an SN progenitor candidate in pre-explosion *HST* archival data using *JWST*, but only by happenstance. The star that exploded as SN 2022acko in NGC 1300 was possibly an RSG with $M_{\text{ini}} \approx 7.7 M_{\odot}$. In our view, the fact that the F814W and F160W detections, considered together, are consistent with an RSG SED, as we would expect for an SN II-P progenitor, is sufficiently compelling to believe that the progenitor has indeed been identified. The inferred M_{ini} of the candidate is slightly below the generally-recognised theoretical juncture at $\sim 8 M_{\odot}$ for core collapse, as opposed to WD formation in less-massive stars. However, this is also just slightly above what the models we considered predict to be an SAGB star, which presumably might end its life as an ECSN. We therefore conclude that SN 2022acko is most likely a normal SN II-P, as all of the observations to be presented forthcoming will show (Bostroem et al., in prep.). The slight discrepancy in our astrometric results, matching the *HST* data to the *JWST* observations and WFC3/IR to WFC/UVIS, is motivation itself for future *HST*

¹ Based on the IRAC zeropoints, 280.9 ± 4.1 and 179.7 ± 2.6 Jy at 3.6 and 4.5 μm , respectively.

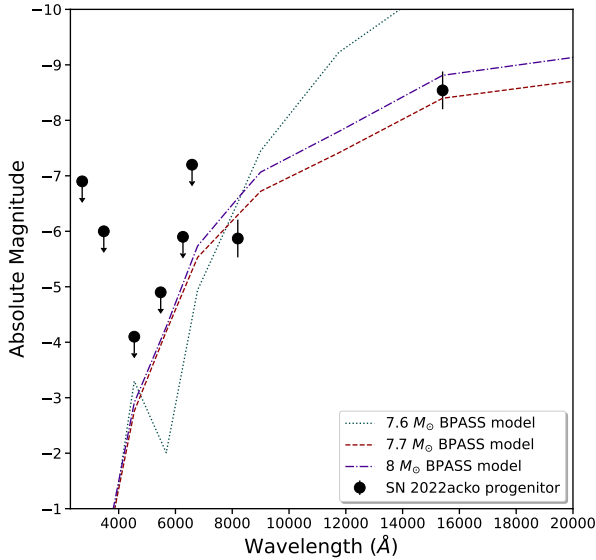


Figure 2. The SN 2022acko progenitor candidate SED, consisting of detections in *HST* F814W and F160W, with 5σ upper limits to detection in several other *HST* bands (see Table 1). The observed photometry has been corrected for an assumed distance of 18.99 ± 2.85 Mpc (Anand et al. 2021) and total visual extinction $A_V = 0.166$ mag (assuming $R_V = 3.1$ for the reddening correction). Also shown are the endpoint SEDs of theoretical single-star models from BPASS v2.2.2 (Stanway & Eldridge 2018) at $M_{\text{ini}} = 7.6, 7.7,$ and $8 M_{\odot}$.

follow-up imaging, when the SN has significantly faded, to confirm that the candidate was indeed the progenitor — although such is good practice, in general, for all progenitor identifications (Van Dyk et al. 2023, and references therein).

With further analysis we do not expect estimates of the interstellar reddening to the SN to evolve by much (all indications are that the total reddening is relatively low); thus, the shape of the progenitor candidate’s SED should not change. However, if a more reliable distance could be measured (e.g., using Cepheids), the overall estimated luminosity of the star could change. We would not expect the luminosity estimate to get any lower (the star already likely sits at the RSG/SAGB boundary); however, a larger distance would only increase the star’s overall luminosity and, consequently, the estimate of its M_{ini} as well.

The present work launches an exciting new avenue for future potential SN progenitor identifications via *JWST*, either through further serendipity or dedicated guest investigator or discretionary observations.

ACKNOWLEDGEMENTS

This work is based in part on observations made with the NASA/ESA *Hubble Space Telescope* obtained from the Space Telescope Science Institute, which is operated by the Association of Universities for Research in Astronomy, Inc., under NASA contract NAS 5-26555. This work is based in part on observations made with the NASA/ESA/CSA *James Webb Space Telescope*. The data were obtained from the Mikulski Archive for Space Telescopes at STScI. This research has made use of the NASA/IPAC Infrared Science Archive, which is

funded by the National Aeronautics and Space Administration and operated by the California Institute of Technology. This publication was made possible through the support of an LSSTC Catalyst Fellowship to K.A.B., funded through grant 62192 from the John Templeton Foundation to LSST Corporation. The opinions expressed in this publication are those of the authors and do not necessarily reflect the views of LSSTC or the John Templeton Foundation. Time-domain research by the University of Arizona team and D.J.S. is supported by NSF grants AST-1821987, 1813466, 1908972, & 2108032, and by the Heising-Simons Foundation under grant #20201864. J.E.A. is supported by the international Gemini Observatory, a program of NSF’s NOIRLab, which is managed by the Association of Universities for Research in Astronomy (AURA) under a cooperative agreement with the National Science Foundation, on behalf of the Gemini partnership of Argentina, Brazil, Canada, Chile, the Republic of Korea, and the United States of America. A.V.F. has received financial assistance from the Christopher R. Redlich Fund, numerous individual donors, and NASA/*HST* grant AR-14259 from STScI. Research by S.V. and Y.D. is supported by NSF grant AST-2008108.

DATA AVAILABILITY

All of the *HST* and *JWST* data analysed herein are publicly available via the Mikulski Archive for Space Telescopes (MAST) portal, <https://mast.stsci.edu/search/ui/#/hst>. All of the *Spitzer* data are publicly available via the NASA/IPAC Infrared Science Archive (IRSA), <https://irsa.ipac.caltech.edu/>. All of the photometric results that we have obtained from these data are listed above.

REFERENCES

- Anand G. S., et al., 2021, *MNRAS*, **501**, 3621
 Anderson J. P., et al., 2014, *ApJ*, **786**, 67
 Brennan S. J., Elias-Rosa N., Fraser M., Van Dyk S. D., Lyman J. D., 2022, *A&A*, **664**, L18
 Davies B., Beasar E. R., 2020, *MNRAS*, **496**, L142
 Davies B., Plez B., Petraut M., 2022, *MNRAS*, **517**, 1483
 Dell’Aglì F., García-Hernández D. A., Schneider R., Ventura P., La Franca F., Valiante R., Marini E., Di Criscienzo M., 2017, *MNRAS*, **467**, 4431
 Doherty C. L., Gil-Pons P., Siess L., Lattanzio J. C., 2017, *Publ. Astron. Soc. Australia*, **34**, e056
 Dolphin A., 2016, DOLPHOT: Stellar photometry, Astrophysics Source Code Library, record ascl:1608.013 (ascl:1608.013)
 Eldridge J. J., Maund J. R., 2016, *MNRAS*, **461**, L117
 Filippenko A. V., 1997, *ARA&A*, **35**, 309
 Gal-Yam A., 2017, in Alsabti A. W., Murdin P., eds., *Handbook of Supernovae*. p. 195, doi:10.1007/978-3-319-21846-5_35
 Gal-Yam A., Leonard D. C., 2009, *Nature*, **458**, 865
 Graur O., Bianco F. B., Modjaz M., Shivvers I., Filippenko A. V., Li W., Smith N., 2017, *ApJ*, **837**, 121
 Hiramatsu D., et al., 2021, *Nature Astronomy*, **5**, 903
 Jencson J. E., Sand D. J., Andrews J. E., Smith N., Strader J., Aghakhanloo M., Pearson J., Valenti S., 2022, *ApJ*, **935**, L33
 Kilpatrick C. D., et al., 2018, *MNRAS*, **480**, 2072
 Kilpatrick C. D., et al., 2021, *MNRAS*, **504**, 2073
 Lee J. C., et al., 2022a, *arXiv e-prints*, p. arXiv:2212.02667
 Lee J. C., et al., 2022b, *ApJS*, **258**, 10
 Li W., Van Dyk S. D., Filippenko A. V., Cuillandre J.-C., Jha S., Bloom J. S., Riess A. G., Livio M., 2006, *ApJ*, **641**, 1060
 Li W., et al., 2011, *MNRAS*, **412**, 1441
 Li L., Cai Y., Zhai Q., Zhang J., Wang X., 2022, Transient Name Server Classification Report, 2022-3549, 1

- Lundquist M., et al., 2022, Transient Name Server Discovery Report, [2022-3543, 1](#)
- Makovoz D., Khan I., 2005, in Shopbell P., Britton M., Ebert R., eds, *Astronomical Society of the Pacific Conference Series Vol. 347, Astronomical Data Analysis Software and Systems XIV*. p. 81
- Makovoz D., Marleau F. R., 2005, [PASP, 117, 1113](#)
- Massey P., Plez B., Levesque E. M., Olsen K. A. G., Clayton G. C., Josselin E., 2005, [ApJ, 634, 1286](#)
- Maund J. R., Smartt S. J., Danziger I. J., 2005, [MNRAS, 364, L33](#)
- Miyaji S., Nomoto K., Yokoi K., Sugimoto D., 1980, [PASJ, 32, 303](#)
- Nomoto K., 1984, [ApJ, 277, 791](#)
- O’Neill D., et al., 2019, [A&A, 622, L1](#)
- O’Neill D., Kotak R., Fraser M., Mattila S., Pietrzyński G., Prieto J. L., 2021, [A&A, 645, L7](#)
- STScI Development Team 2012, DrizzlePac: HST image software, Astrophysics Source Code Library, record ascl:1212.011 (ascl:1212.011)
- Shaya E. J., Tully R. B., Hoffman Y., Pomarède D., 2017, [ApJ, 850, 207](#)
- Smartt S. J., 2015, [Publ. Astron. Soc. Australia, 32, e016](#)
- Smartt S. J., Eldridge J. J., Crockett R. M., Maund J. R., 2009, [MNRAS, 395, 1409](#)
- Smith N., Li W., Filippenko A. V., Chornock R., 2011, [MNRAS, 412, 1522](#)
- Smith N., Andrews J. E., Filippenko A. V., Fox O. D., Mauerhan J. C., Van Dyk S. D., 2022, [MNRAS, 515, 71](#)
- Stanway E. R., Eldridge J. J., 2018, [MNRAS, 479, 75](#)
- Tartaglia L., et al., 2018, [ApJ, 853, 62](#)
- Valenti S., et al., 2016, [MNRAS, 459, 3939](#)
- Van Dyk S. D., 2017, *Philosophical Transactions of the Royal Society of London Series A*, [375, 20160277](#)
- Van Dyk S. D., et al., 2012, [AJ, 143, 19](#)
- Van Dyk S. D., et al., 2018, [ApJ, 860, 90](#)
- Van Dyk S. D., et al., 2019, [ApJ, 875, 136](#)
- Van Dyk S. D., et al., 2023, [MNRAS, 519, 471](#)
- Woosley S. E., Weaver T. A., 1986, [ARA&A, 24, 205](#)
- Xiang D., et al., 2019, [ApJ, 871, 176](#)
- Zhang J., et al., 2020, [MNRAS, 498, 84](#)
- de Jaeger T., et al., 2019, [MNRAS, 490, 2799](#)

This paper has been typeset from a $\text{\TeX}/\text{\LaTeX}$ file prepared by the author.